Photodissociation of nitromethane cluster anions

Daniel J. Goebbert, Dmitry Khuseynov, and Andrei Sanov[a)]
Department of Chemistry and Biochemistry, University of Arizona, Tucson, Arizona 84721-0041, USA

(Received 14 June 2010; accepted 25 July 2010; published online 31 August 2010)

Three types of anionic fragments are observed in the photodissociation of nitromethane cluster anions, $(CH_3NO_2)_n^-$, $n=1-6$, at 355 nm: $NO_2^-(CH_3NO_2)_k$, $(CH_3NO_2)_k^-$, and OH^- $(k<n)$. The fragmentation trends are consistent with the parent clusters containing a monomer-anion core, $CH_3NO_2^-$, solvated by $n-1$ neutral nitromethane molecules. The $NO_2^-(CH_3NO_2)_k$ and OH^- fragments formed from these clusters are described as core-dissociation products, while the $(CH_3NO_2)_k^-$ fragments are attributed to energy transfer from excited $CH_3NO_2^-$ into the solvent network or a core-dissociation—recombination (caging) mechanism. As with other cluster families, the fraction of caged photofragments shows an overall increase with increasing cluster size. The low-lying A^2A' and/or B^2A' electronic states of $CH_3NO_2^-$ are believed responsible for photoabsorption leading to dissociation to NO_2^- based fragments, while the C^2A'' state is a candidate for the OH^- pathway. Compared to neutral nitromethane, the photodissociation of $CH_3NO_2^-$ requires lower energy photons because the photochemically active electron occupies a high energy π^* orbital (which is vacant in the neutral). Although the electronic states in the photodissociation of CH_3NO_2 and $CH_3NO_2^-$ are different, the major fragments, CH_3+NO_2 and $CH_3+NO_2^-$, respectively, both form via C–N bond cleavage. © *2010 American Institute of Physics*. [doi:10.1063/1.3479586]

I. INTRODUCTION

Nitromethane, CH_3NO_2, is known for its rich and complex chemistry, which is largely due to the nitro group. The unique properties of this substituent are dictated by the electronegative nature of the constituent atoms, a large molecular dipole moment, and a resonant π system interacting with the nonbonding lone pairs of electrons on the oxygen atoms. An important property of nitromethane (NM) is its propensity to form negative ions in the gas phase by electron attachment.[1–6] The mechanism of electron attachment to NM has been studied using a number of techniques, primarily involving collisions with electrons, alkali, or high-Rydberg atoms.[1–5] The reverse process, electron detachment from NM^-, has also been studied in detail by negative-ion photoelectron spectroscopy.[3,7,8]

These experiments have revealed that electron attachment to NM forms valence NM^- anion via an initial electron-molecule complex, a gateway dipole-bound state that involves a diffuse Rydberg-type orbital protruding from the CH_3 group. In the neutral and dipole-bound anionic states, the $C-NO_2$ group is nearly planar, but in the valence-bound anion these atoms are found in a nonplanar arrangement, with the nitrogen at the apex of a pyramidal structure. Theoretical studies have suggested that in the neutral CH_3NO_2 molecule distortion from the planar $C-NO_2$ structure stabilizes the vacant π^* orbital on the NO_2 group. In the anionic form, distortion from the planar arrangement localizes the electron in this π^* orbital, yielding the valence anion.[1,3,9]

Electron collision experiments have shown that nitromethane not only forms anions but also undergoes anionic fragmentation. Recent studies investigated dissociative electron attachment to NM over a range from 0 to 16 eV.[10,11] The major fragments observed were NO_2^-, O^-, OH^-, CN^-, and CNO^-, along with several minor products: $CH_2NO_2^-$, $CHNO_2^-$, CH_2NO^-, H_2NO^-, CH_3^-, CH_2^-, CH^-, and H^-. Most of the fragment anions were observed at electron collision energies between 5 and 10 eV and had low relative intensities, but two important fragments had noticeably different appearance energies: NO_2^-, with a maximum intensity at around 0.62 eV, and OH^-, which had a pronounced maximum near 0 eV. Most fragmentation channels are believed to occur via dissociative electron attachment, but OH^- is thought to form via a bimolecular process.

Little is known about cluster anions containing nitromethane. Wincel[12] measured the solvation energies of NM^- containing clusters, and binding energies of several other anions solvated by NM. Another study focused on the photodissociation of $X^-\cdot NM$ (X=I or Br) clusters and three types of fragment ions, X^-, NM^-, and NO_2^-, were observed by photofragment action spectroscopy.[13] For the $I^-\cdot NM$ cluster, the NM^- fragment was most intense at photon energies of 3.59 eV. The I^- and NO_2^- fragments also had sharp peaks at 3.59 eV, but exhibited additional structure at higher photon energies, corresponding to excitation of the $-NO_2$ vibrations. In the ground state of the $X^-\cdot NM$ clusters, the excess electron is localized on the halogen atoms, while the nitromethane molecules play the role of (neutral) solvent. The mechanism for formation of either X^- or NO_2^- photofragments in these systems can be interpreted in a manner similar to an S_N2 reaction. A more recent study of hydrated NM^- showed typical stepwise increases in electron binding energy, until $NM^-(H_2O)_6$, which showed a low-energy feature attrib-

a)Electronic mail: sanov@u.arizona.edu.

uted to a "dual dipole-bound" anion. Photofragmentation of the clusters at 2134 nm indicated that the dipole bound $NM^-(H_2O)_6$ was converted to a valence-bound fragment $NM^-(H_2O)_3$.[14]

Although NM^- is a relatively small molecule, it has proven to be a challenging system for electronic structure calculations. The difficulty of obtaining reliable theoretical descriptions of NM^- is highlighted in a comprehensive theoretical study of the electron affinity of NM, where various levels of theory give values ranging from −0.126 to 0.595 eV,[15] compared to the experimental result of 0.172 ± 0.006 eV.[7] Theoretical studies have examined direct dissociation of $CH_3NO_2^-$ to $CH_3+NO_2^-$.[16,17] The dissociation barrier was calculated to be 0.35 eV,[16] but a more recent study placed the barrier height at about 0.78 eV.[17] The potential isomerization to CH_3ONO^- with subsequent fragmentation to CH_3O^-+NO has also been explored and found to be much less favorable. The ground state of $CH_3NO_2^-$ is $^2A'$, while that of CH_3ONO^- is $^2A''$ so the transformation is nonadiabatic. On the $^2A''$ surface, the rearrangement involves a large potential barrier, calculated to be 2.59 eV.[16] Furthermore, another study questioned the stability of the CH_3ONO^- isomerization product, as some levels of theory predict an unstable isomer.[17]

In this paper, we report several fragmentation processes in the photodissociation of nitromethane cluster anions, $(NM)_n^-$, $n=1-6$, at 355 nm. In contrast to the past work on $X^-\cdot NM$ clusters,[13] the charge in $(NM)_n^-$ is localized on a NM molecule; hence, nitromethane plays the dual role of an anionic solute and neutral solvent. The photochemistry of the core anion, NM^-, is due to the excess electron occupying the antibonding π^* orbital. Transition energies from this orbital to other low-energy antibonding orbitals are lower compared to transitions in neutral NM, which involve nonbonding or π electrons. At 355 nm, the photochemistry of $(NM)_n^-$ is initiated by photoabsorption by the core anion, NM^-, without competing dissociation of neutral NM molecules. The dominant NM^- dissociation process is the breaking of the C–N bond to yield the $NO_2^-+CH_3$ products.[17] These products are analogous to those in the photodissociation of neutral NM at 271–193 nm, where photon energies are sufficient to initiate the dissociation process in the neutral.[18–22]

II. EXPERIMENTAL AND THEORETICAL METHODS

The experiments were performed using a tandem time-of-flight reflectron mass-spectrometer described in detail elsewhere.[23] Cluster anions are generated in a pulsed (50 Hz) supersonic expansion of nitromethane vapor in Ar carrier gas with a backing pressure of 20 psi. The expansion is crossed with a 1 keV electron beam, which produces slow electrons from collisions with the gas. The desired cluster anions are formed by dissociative attachment of slow secondary electrons to neutral nitromethane clusters. A Wiley–McLaren time-of-flight mass spectrometer separates the ions according to their mass-to-charge ratio. The third harmonic (355 nm, 20 mJ/pulse) of a Nd:YAG (yttrium aluminum garnet) laser (Quanta Ray, Laboratory 50, 8 ns pulse duration) intersects the ions prior to the reflectron stage. Fragment ions are detected by scanning the reflectron potential while monitoring the ion intensity with a dual microchannel plate detector. Typically, 512 mass-spectral traces are averaged for each fragment ion. The mass-spectra reported in this work are composites of the scanning steps.

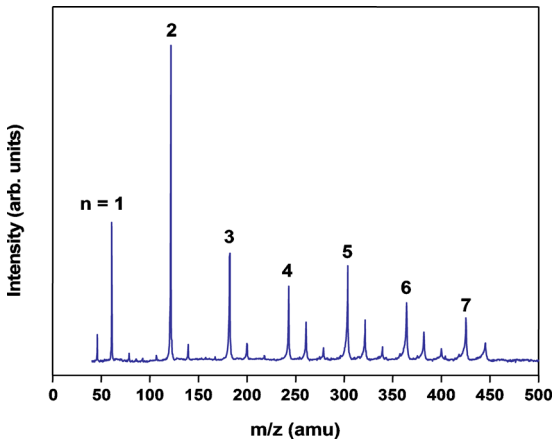

FIG. 1. Representative time-of-flight mass spectrum of parent ions formed by electron attachment to NM clusters in the ion source. The major $(NM)_n^-$ peaks are labeled. Other peaks correspond to hydrated ions and $NO_2^-(NM)_n$ clusters.

Electronic structure calculations were carried out with the GAUSSIAN 03 suite of programs,[24] using density functional theory with the 6-311++G(3df,3pd) basis set. The geometry of the anion in the ground state was optimized and normal mode analysis confirmed that the structure found was indeed a stationary point (all frequencies were real). Excited states were treated at the optimized geometry of the anion, either explicitly or by using the time-dependent density functional theory (TD-DFT) approach.[25–27]

III. RESULTS

A representative time-of-flight mass spectrum of the parent anions formed by electron attachment to nitromethane clusters is shown in Fig. 1. The nitromethane cluster anions, $(NM)_n^-$, are the dominant species observed. The $m/z=46$ peak, just below the $n=1$ peak, is assigned to NO_2^-, while most of the low-intensity peaks neighboring the intense $(NM)_n^-$ peaks correspond to hydrated clusters. The most intense peak in the spectrum corresponds to the dimer anion, $(CH_2NO_2)_2^-$, followed by the monomer anion, $CH_2NO_2^-$, while the larger clusters steadily decrease in intensity with increasing size. The formation of NO_2^- from dissociative electron attachment is consistent with the previous electron attachment studies of NM, where NO_2^- was the major fragment ion observed even at low electron kinetic energies.[10,11] Clusters of NO_2^- with NM have negligible intensity in our primary (parent-ion) mass-spectra.

The 355 nm photofragment-ion mass spectra for $(NM)_n^-$, $n=1-6$, are shown in Fig. 2. With increasing parent cluster size, n, the maximum of the fragment intensity distribution shifts to higher-mass fragments. The dominant fragments observed for the smaller clusters are described by the general formula $NO_2^-(NM)_k$, while the larger clusters preferentially form the $(NM)_k^-$, $k<n$, fragment ions.

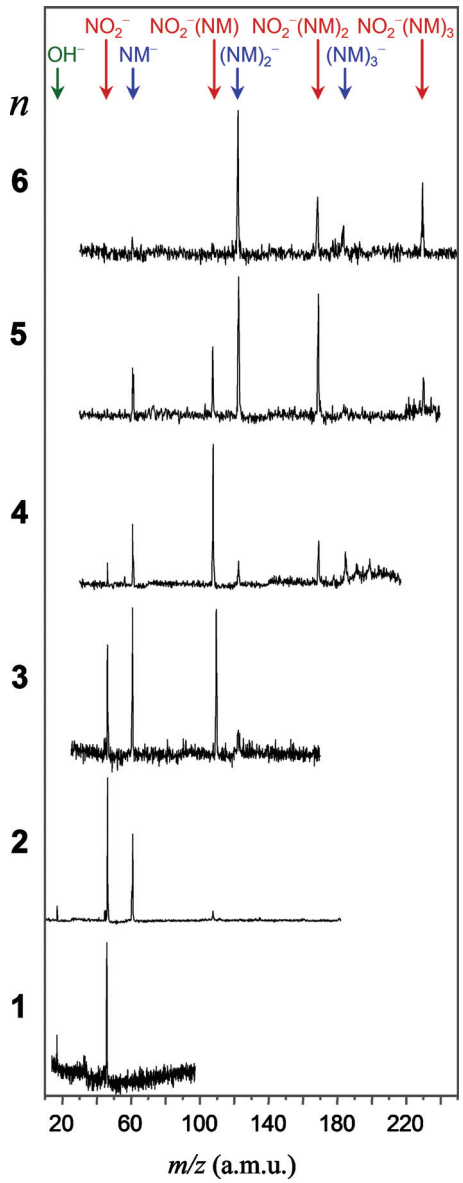

FIG. 2. 355 nm photodissociation mass spectra of $(NM)_n^-$, $n=1-6$. Peak assignments are indicated along the top of the figure, where the green arrow represents OH^-, red labels are for $NO_2^-(NM)_k$ fragments, and blue labels show the $(NM)_k^-$ species.

The observed photofragments suggest the following reaction pathways:

$$(NM)_n^- + h\nu \rightarrow (n-k-1)NM + CH_3 + NO_2^-(NM)_k \quad (1)$$

$$\rightarrow (n-1)NM + CH_2NO + OH^- \quad (2)$$

$$\rightarrow (n-k)NM + (NM)_k^-. \quad (3)$$

All of these pathways are energetically accessible in the photodissociation of $(NM)_n^-$ with 3.5 eV photons. The mass-spectral peaks corresponding to the anionic photofragments formed via these pathways are labeled in Fig. 2. The first process [Eq. (1), red labels in Fig. 2] implies dissociation of NM^- within $(NM)_n^-$ to produce NO_2^-, which may remain associated with additional NM solvent molecules. The second reaction [Eq. (2), green label in Fig. 2] is the formation of OH^-. This fragment is observed only for the NM^- and $(NM)_2^-$ parent ions. Solvated OH^- fragments are not seen in quantities sufficient for unambiguous identification. The third type of fragmentation reaction is NM solvent evaporation [Eq. (3), blue labels in Fig. 2].

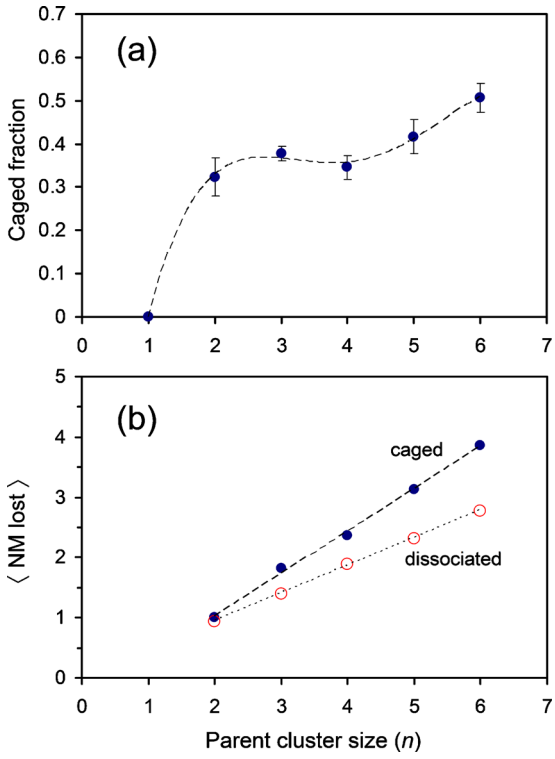

FIG. 3. Cluster size dependent trends for (a) the fraction of $(NM)_k^-$ (caged) products, and (b) the average number of NM molecules lost within the caged and core-dissociated products (closed and open circles, respectively), as functions of parent cluster size, n. The dashed curve in (a) is a polynomial fit to the data intended to guide the eye. The dashed lines in (b) represent linear regressions of the corresponding data sets.

We will refer to the anionic fragments formed via Eqs. (1) and (2) as core-dissociation fragments, while the $(NM)_k^-$ ions formed via Eq. (3) will be described as "caged" photofragments. The fractional yield of the caged photoproducts tends to increase with increasing size of the parent $(NM)_n^-$ clusters. The combined yield of all $(NM)_k^-$ fragments, relative to the total anionic fragment yield, is plotted in Fig. 3(a) as a function of the parent cluster size, n. The values shown were obtained by integrating the corresponding fragment peak intensities. The fractional yield of the caged fragments reaches about a half for $n=6$. By analogy with the trends seen in other cluster systems,[28–34] one expects the caged fragment fraction to increase further for larger $(NM)_n^-$ clusters.

Figure 3(b) shows ⟨NM lost⟩, the average numbers of (intact) neutral NM molecules evaporated in the core-dissociated and caged photofragments, respectively, also plotted versus the parent cluster size, n. In calculating ⟨NM lost⟩ for the core-dissociation channels, the number of evaporated NM in Eqs. (1) and (2) equals $(n-k-1)$ and $(n-1)$, respectively. For caged fragments, the quantity plotted represents the average of $(n-k)$, per Eq. (3). The ⟨NM lost⟩ values for both the caged and core-dissociated channels display approximately linear trends, increasing with n, but are generally lager for the caged fragments.

IV. DISCUSSION

A. Dissociation mechanisms

1. Overview

We will show that the experimental observations are consistent with each $(NM)_n^-$ cluster having a NM^- core anion, i.e., the cluster structures are best described as $NM^-(NM)_{n-1}$. It is the NM^- cluster core that absorbs the excitation photon. Past work revealed no evidence of stable (electron-bound) excited states of NM^-.[8] Therefore, the excitation of bare NM^- results either in direct photodetachment or in excitation of an anionic resonance $[NM^-]^*$, which may, in turn, decay by either autodetachment or fast dissociation. In clusters, $[NM^-]^*$ may be stabilized by solvation, decreasing the probability of autodetachment in favor of solvent-enabled chemistry.[35] Focusing on the anionic fragmentation channels, $[NM^-]^*$ is expected to yield the dominant $CH_3+NO_2^-$ fragments. In clusters, the $CH_3+NO_2^-$ photofragment recombination (caging)[28,29,36,37] may occur or, alternatively, $[NM^-]^*$ may relax via direct energy transfer to the solvent network. Both processes will be followed by NM solvent evaporation, resulting in the overall reaction described by Eq. (3).

It is instructive to compare the photodissociation of NM^- to that of neutral nitromethane. A number of groups have studied the vacuum-UV (~271–193 nm) photodissociation of this molecule.[18–22] Recent theoretical studies have suggested the excited state decays through a S_3/S_2 conical intersection, which ultimately yields the NO_2+CH_3 products.[38] In the present study, we observed a similar dissociation, specifically, cleavage of the C–N bond in NM^-. Neutral OH formation, which would be analogous to the OH^- channel in the anion, has not been seen in NM dissociation. (Instead, the CH_3O+NO rearrangement products were observed in infrared multiphoton dissociation studies.[39])

2. Electronic states

Compared to neutral NM, electronic excitation of the anion and, consequently, NM^- dissociation can be induced with lower energy photons. In the X^2A' ground state of NM^-, the unpaired electron occupies the π^* (11a′) orbital localized primarily on the nitro group.[8] Thus, in contrast to the photodissociation of neutral NM, which occurs via the $\pi^*(NO_2) \leftarrow \pi(NO_2)$ or $\pi^*(NO_2) \leftarrow \sigma(CN)$ transitions,[40] the π^* orbital is occupied in the anion and it is this unpaired electron that is photochemically active in our study. The relatively high energy of this orbital is responsible for the smaller electronic excitation gaps in the anion, while its π^* character leads to a nonplanar anion structure and a slight increase of the NO_2 bond lengths in NM^-, compared to NM.

The three lowest-energy, same-spin unoccupied orbitals at the equilibrium geometry of NM^- are 12a′, 13a′, and 7a″, as indicated by the UB3LYP/6-311++G(3df,3pd) calculations. Excitation of the 11a′ electron to one of these orbitals yields the A^2A', B^2A', and C^2A'' excited states, respectively. The 12a′ and 13a′ orbitals both have some antibonding σ^* character along the C–N bond; hence, the A^2A' and/or B^2A' states are expected to be important in NM^- dissociation to $CH_3+NO_2^-$. On the other hand, 7a″ is a C–H σ^* type orbital; the C^2A'' state may, therefore, play a role in the OH^- fragment formation.

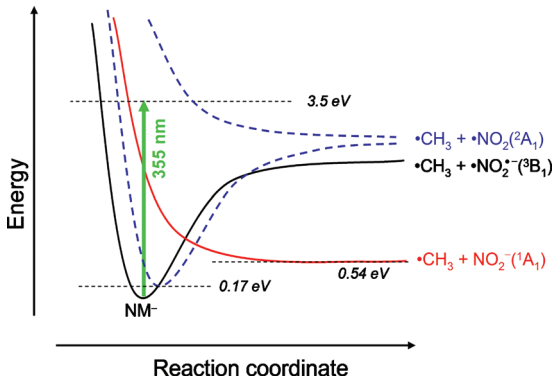

FIG. 4. Schematic potential energy curves for the dissociation of NM^- into CH_3 and NO_2^-. The energy scale is not linear. Direct dissociation along the C–N bond yields NO_2^- with two unpaired electrons, indicated as $\bullet NO_2^{\bullet -}$, in the $^3B_1$ state (black curve). The ground state of NO_2^-, $^1A_1$, is lower in energy and corresponds to the repulsive dissociation curve shown in red. The ground and dissociative states of neutral NM are indicated by the dashed blue lines.

To gain insight into the roles of NM^- excited states in photodissociation, we surveyed the energy differences between the ground and excited electronic states using several theoretical methods. Within a one-electron Koopman's theorem approach, the vertical transition energies between the 11a′ HOMO and the 12a′, 13a′, and 7a″ orbitals of the anion were estimated at 1.66, 2.58, and 2.69 eV, respectively. Alternatively, the TD-DFT method yields transition energies of 1.02, 1.83, and 1.98 eV, corresponding to the A^2A', B^2A', and C^2A'' excited states, respectively. This method also predicts the oscillator strengths for the A^2A' and B^2A' states to be much larger than that for the C^2A'' state. The C^2A'' state energy could be calculated explicitly because it involves electron promotion to an orbital of different symmetry. The calculation yielded 2.37 eV for the $X \rightarrow C$ vertical transition energy. As the large discrepancies between the computed values illustrate, excited states are notoriously difficult to model; however, the qualitative predictions are still useful. To set the accuracy of the above predictions in an experimental perspective, we attempted photodissociation of NM^- and $(NM)_2^-$ at 532 nm (2.33 eV) and did not observe any anionic fragments. This suggests that the dissociative excited states lie >2.33 eV (vertically) above the NM^- minimum.

3. $CH_3NO_2^- \rightarrow CH_3+NO_2^-$

In a recent study of collisions between oriented nitromethane molecules with sodium atoms, qualitative potential energy curves were used to explain the mechanism of $CH_3+NO_2^-$ formation.[1,2] A repulsive $^2A'$ potential was proposed to play a primary role in dissociative electron transfer. This state would correlate with the electronic ground states of the CH_3 and NO_2^- fragments. Building on this work, in Fig. 4 we show qualitative potential energy curves for NM^- dissociation, based primarily on our findings. Direct cleavage of the C–N bond in the ground electronic state of the anion yields CH_3 and NO_2^-, but this NO_2^- fragment is in the ex-

cited $^3B_1$ state. The ground state of NO_2^- is $^1A_1$, in which all electrons are paired, while the ground state of CH_3 is $^2A_2''$. Since covalent bond formation between the fragments in these states is not possible, the $NO_2^-(X^1A_1)+CH_3(X^2A_2'')$ potential is repulsive.

The excited states of the methyl radical are much higher in energy and can safely be ignored in this discussion, while the adiabatic difference between the X^1A_1 and a $^3B_1$ states of NO_2^-, calculated at the UB3LYP/6-311++G(3df,3pd) theory level, is 1.95 eV. This value corresponds to the gap between the two anion curves in the asymptotic limit in Fig. 4. The adiabatic C–N dissociation energy of NM^- can be calculated using the following thermochemical cycle:

$$\begin{array}{lll} CH_3NO_2^- \rightarrow CH_3NO_2 + e^- & EA(CH_3NO_2) = 0.172\ \text{eV} & (\text{Ref. } 7) \\ CH_3NO_2 \rightarrow CH_3 + NO_2 & BDE = 2.64\ \text{eV} & (\text{Ref. } 41) \\ NO_2 + e^- \rightarrow NO_2^- & -EA(NO_2) = -2.273\ \text{eV} & (\text{Ref. } 42) \\ \hline CH_3NO_2^- \rightarrow CH_3 + NO_2^- & BDE = 0.54\ \text{eV} & \end{array} \quad (4)$$

The resulting $BDE(H_3C–NO_2^-)=0.54$ eV is indicated in Fig. 4. We also show in Fig. 4 the potential minimum for neutral NM, which lies 0.172 eV above NM^-,[7] and the repulsive excited state for photodissociation of NM to CH_3 and NO_2, which lies (vertically) beyond the 3.5 eV photon energy used in our experiment. In the fragment limit, UB3LYP/6-311++G(3df,3pd) calculations set $NO_2(X^2A_1)$ 2.23 eV above $NO_2^-(X^1A_1)$, in good agreement with the 2.273 eV experimental value of adiabatic electron affinity of NO_2.[42]

It follows from the diagram in Fig. 4 that dissociation to CH_3 and NO_2^- on the repulsive $[NM^-]^*$ surface is possible, provided that the fragments separate rapidly beyond the crossing of the neutral and anion potential curves. Since we observe these anionic fragments experimentally and no major autodetachment features are present in the photoelectron spectrum of NM^- at 355 nm,[8] the dissociation must indeed be faster than autodetachment. This is reasonable because the timescale for autodetachment in this case is expected to be longer than that of dissociation on a repulsive potential.[43,44]

4. $CH_3NO_2^- \rightarrow OH^- + CH_2NO$

Formation of OH^- was previously reported in dissociative electron attachment to nitromethane, with a sharp onset near zero electron kinetic energy.[4,10,11] In our experiment, OH^- is formed in low relative intensity in photodissociation of NM^- and $(NM)_2^-$. The corresponding rearrangement process may occur in either the ground or one of the excited electronic states of NM^-. In particular, the C^2A'' state corresponds to a C–H $\sigma^* \leftarrow \pi^*$ excitation, which may be responsible for the C–H bond cleavage necessary for the formation of OH^- from $CH_3NO_2^-$. Previous theoretical results have also shown a small amount of σ^* character on the methyl group in the HOMO of NM^-, suggesting that the C–H bonds may be slightly weakened in the anion.[7] Our calculations agree with the earlier studies, and we find that the C–H bonds are slightly longer in NM^- compared to NM, a likely indication of a weaker bond.

The possibility of the $CH_3NO_2^- \rightarrow OH^- + CH_2NO$ reaction in the ground electronic state should also be considered. In Fig. 5, we show the energetics for this reaction, calculated at the B3LYP/6-311++G(3df,3pd) level of theory. We find that the reaction leads directly to the $OH^- + CH_2NO$ products, with no stable intermediate structure. The transition state is calculated to be 1.83 eV higher in energy than $CH_3NO_2^-$, well within the energy available due to photon absorption, but much larger than the energies for electron detachment or solvent evaporation. The products energy is about 1.03 eV higher relative to $CH_3NO_2^-$.

B. Solvation effects

The solvent evaporation (binding) energies for $(NM)_n^- \rightarrow (NM)_{n-1}^- + NM$, determined in a previous experiment,[12] are listed in Table I. The binding energy of $(NM)_6^- \rightarrow (NM)_5^- + NM$ was not measured, but the values for $n<6$ show a linear trend versus cluster size and extrapolating the available data to $n=6$ provides an estimate of the binding energy of approximately 0.26 eV. Combining the sequential solvation energies, the complete solvent evaporation energy

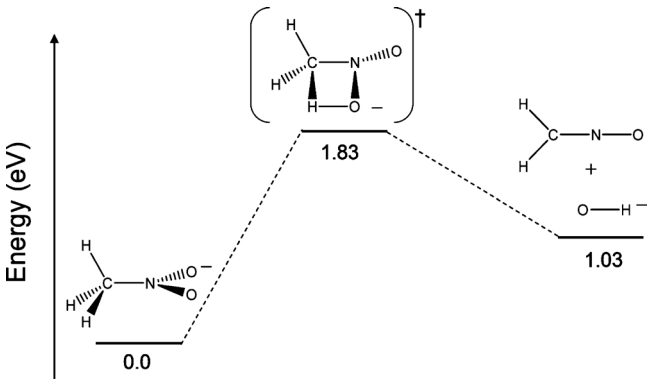

FIG. 5. Reaction profile for formation of OH^- from $CH_3NO_2^-$, calculated at the B3LYP/6-311++G(3df,3pd) level of theory. The transition state corresponds to formation of a four-membered intermediate which leads to direct loss of OH^-.

TABLE I. Relevant reaction energetics.

Reaction	Energy (eV)	Reference
$(NM)_2^- \rightarrow NM + NM^-$	0.659 ± 0.009	12
$(NM)_3^- \rightarrow NM + (NM)_2^-$	0.556 ± 0.013	12
$(NM)_4^- \rightarrow NM + (NM)_3^-$	0.451 ± 0.022	12
$(NM)_5^- \rightarrow NM + (NM)_4^-$	0.364 ± 0.009	12
$(NM)_6^- \rightarrow NM + (NM)_5^-$	0.26[a]	This work
$NM^- \rightarrow NM + e^-$	0.171 ± 0.006	7
$CH_3NO_2 \rightarrow CH_3 + NO_2$	2.640	41
$NO_2^- \rightarrow NO_2 + e^-$	2.2730 ± 0.0050	42
$CH_3NO_2^- \rightarrow CH_3 + NO_2^-$	0.54[b]	This work

[a]Estimated from linear extrapolation of dissociation energies (see text).
[b]Per Eq. (4).

from the largest cluster in the present study, $(NM)_6^- \rightarrow 5NM + NM^-$, can be calculated to be approximately 2.3 eV.

Taking into account the 3.5 eV photon energy, there is sufficient energy to completely remove all solvent molecules from the largest cluster anion investigated in this study. Including the additional 0.54 eV for NM^- dissociation [per Eq. (4)], complete solvent evaporation *and* core-dissociation of $(NM)_6^-$ to yield an unsolvated NO_2^- requires about 2.8 eV. Although this is less than the 3.5 eV photon energy, no bare NO_2^- fragments are observed from $(NM)_6^-$, or even $(NM)_5^-$. However, these parent clusters do yield $NO_2^-(NM)_k$, $0 < k < n$. The largest parent cluster for which the unsolvated NO_2^- fragments are unambiguously detected is $(NM)_4^-$ (see Fig. 2).

If we compare the binding energies in Table I to the dissociation energy of NM^-, we find that NM^- core-dissociation is energetically more favorable compared to solvent evaporation for $(NM)_2^-$ and $(NM)_3^-$, assuming the dissociation energy is largely unaffected by solvation. This is consistent with the intense $NO_2^-(NM)_k$ fragments observed for $(NM)_2^-$ and $(NM)_3^-$. The first solvent evaporation for $(NM)_4^-$, however, is slightly lower in energy compared to NM^- core-dissociation. Therefore, based on the relative energies alone we might expect a shift toward caged fragments (pure solvent evaporation) for $(NM)_n^-$, $n \geq 4$. At the same time, from a mechanistic point of view, since caging occurs via energy transfer from $[NM^-]^*$ to the solvent system, its probability is expected to increase when the core anion is surrounded by a large number of solvent molecules. This expectation is in agreement with the caging probability trend seen in Fig. 3(a).

As seen in Fig. 3(b), more solvent NM molecules are evaporated from the clusters in the caged product channels, compared to the core-dissociated pathways. This is because the energy available for solvent evaporation in the latter case is reduced by the amount spent on dissociating the core anion bond. Although no asymptotic convergence is achieved in Fig. 3(b) within the cluster size-range studied, the difference in $\langle NM\ lost \rangle$ between the caged and core-dissociated products, $\Delta\langle NM\ lost \rangle$, is ~ 1 for $n = 5-6$. Consulting Table I, $\Delta\langle NM\ lost \rangle$ of ~ 1 corresponds to roughly 0.5 eV in solvent evaporation energy—comparable to the adiabatic C–N BDE of NM^-.

V. CONCLUSIONS AND FUTURE DIRECTIONS

We presented a study of the photodissociation of the $(NM)_n^-$, $NM = CH_3NO_2$, $n = 1-6$, cluster anions at 355 nm. Three types of fragmentation processes are observed, giving rise to the $NO_2^-(NM)_k$, OH^-, and $(NM)_k^-$, $k < n$, anionic fragments. The results are consistent with the model of $(NM)_n^-$ clusters involving a monomer-anion NM^- core, as implied by a $NM^-(NM)_{n-1}$ structure. The $NO_2^-(NM)_k$ and OH^- fragments formed from these clusters are described as core-dissociation products. The $(NM)_k^-$ fragments, on the other hand, are attributed to energy transfer from an initially excited $CH_3NO_2^-$ into the solvent network or a core-dissociation—recombination (caging) mechanism. As with other, previously studied cluster families, the fraction of caged photofragments shows an overall increase with increasing cluster size. The low-lying A^2A' and/or B^2A' electronic states of the core NM^- anion are believed responsible for photoabsorption leading to dissociation to NO_2^- based fragments. The C^2A'' state of NM^- is likely responsible for the OH^- pathway.

Further study of $(NM)_n^-$ dissociation is necessary to extend the range to larger clusters ($n > 6$). As with other strongly solvated cluster systems,[28,30,31,33,34] we expect the caging fraction to approach 1 in the limit of large clusters. Similarly, the $\langle NM\ lost \rangle$ versus n trends [Fig. 3(b)] for both caged and core-dissociated channels is expected to plateau in the limit of large n. These anticipated results will provide insight into the structural motifs and energetics of the $(NM)_n^-$ clusters, illuminating the transition to "bulk" properties.[33,45,46] In addition, wavelength dependent photoexcitation may reveal direct signatures of resonances in the photodissociation spectrum and thus illuminate the dissociation mechanism. Calculations of cluster structures will be helpful in examining the detailed intermolecular interactions controlling fragmentation and photodetachment dynamics.

ACKNOWLEDGMENTS

This work was funded by the U.S. National Science Foundation under Grant No. CHE-0713880.

[1] P. R. Brooks, P. W. Harland, and C. E. Redden, J. Am. Chem. Soc. **128**, 4773 (2006).
[2] P. R. Brooks, P. W. Harland, and C. E. Redden, J. Phys. Chem. A **110**, 4697 (2006).
[3] R. N. Compton, H. S. Carman, C. Desfrancois, H. Abdoulcarmine, J. P. Schermann, J. H. Hendricks, S. A. Lyapustina, and K. H. Bowen, J. Chem. Phys. **105**, 3472 (1996).
[4] I. C. Walker and M. A. D. Fluendy, Int. J. Mass. Spectrom. **205**, 171 (2001).
[5] J. A. Stockdale, F. J. Davis, R. N. Compton, and C. E. Klots, J. Chem. Phys. **60**, 4279 (1974).
[6] R. N. Compton, P. W. Reinhardt, and C. D. Cooper, J. Chem. Phys. **68**, 4360 (1978).
[7] C. L. Adams, H. Schneider, K. M. Ervin, and J. M. Weber, J. Chem. Phys. **130**, 074307 (2009).
[8] D. J. Goebbert, K. Pichugin, and A. Sanov, J. Chem. Phys. **131**, 164308 (2009).
[9] T. Sommerfeld, Phys. Chem. Chem. Phys. **4**, 2511 (2002).
[10] E. Alizadeh, F. Ferreira da Silva, F. Zappa, A. Mauracher, M. Probst, S. Denfil, A. Bacher, T. D. Maerk, P. Limao-Viera, and P. Scheier, Int. J. Mass. Spectrom. **271**, 15 (2008).
[11] W. Sailer, A. Pelc, S. Matejcik, E. Illenberger, P. Scheier, and T. D. Maerk, J. Chem. Phys. **117**, 7989 (2002).

[12] H. Wincel, Int. J. Mass. Spectrom. **226**, 341 (2003).
[13] C. E. H. Dessent, J. Kim, and M. A. Johnson, Faraday Discuss. **115**, 395 (2000).
[14] R. Nakanishi and T. Nagata, J. Chem. Phys. **130**, 224309 (2009).
[15] J. N. Bull, R. G. A. R. Maclagan, and P. W. Harland, J. Phys. Chem. A **114**, 3622 (2010).
[16] G. L. Gutsev, P. Jena, and R. J. Bartlett, J. Chem. Phys. **110**, 403 (1999).
[17] J. F. Arenas, J. C. Otero, D. Pelaez, J. Soto, and L. Serrano-Andres, J. Chem. Phys. **121**, 4127 (2004).
[18] Y. Q. Guo, A. Bhattacharya, and E. R. Bernstein, J. Phys. Chem. A **113**, 85 (2009).
[19] L. J. Butler, D. Krajnovich, Y. T. Lee, G. Ondrey, and R. Bersohn, J. Chem. Phys. **79**, 1708 (1983).
[20] H. S. Kwok, G. Z. He, R. K. Sparks, and Y. T. Lee, Int. J. Chem. Kinet. **13**, 1125 (1981).
[21] D. B. Moss, K. A. Trentelman, and P. L. Houston, J. Chem. Phys. **96**, 237 (1992).
[22] N. C. Blais, J. Chem. Phys. **79**, 1723 (1983).
[23] L. Velarde, T. Habteyes, and A. Sanov, J. Chem. Phys. **125**, 114303 (2006).
[24] M. J. Frisch, G. W. Trucks, H. B. Schlegel *et al.*, GAUSSIAN 03, Gaussian, Inc., Wallingford CT, 2004.
[25] R. E. Stratmann, G. E. Scuseria, and M. J. Frisch, J. Chem. Phys. **109**, 8218 (1998).
[26] R. Bauernschmitt and R. Ahlrichs, Chem. Phys. Lett. **256**, 454 (1996).
[27] M. E. Casida, C. Jamorski, K. C. Casida, and D. R. Salahub, J. Chem. Phys. **108**, 4439 (1998).
[28] M. E. Nadal, P. D. Kleiber, and W. C. Lineberger, J. Chem. Phys. **105**, 504 (1996).
[29] V. Vorsa, P. J. Campagnola, S. Nandi, M. Larsson, and W. C. Lineberger, J. Chem. Phys. **105**, 2298 (1996).
[30] V. Vorsa, S. Nandi, P. J. Campagnola, M. Larsson, and W. C. Lineberger, J. Chem. Phys. **106**, 1402 (1997).
[31] S. Nandi, A. Sanov, N. Delaney, J. Faeder, R. Parson, and W. C. Lineberger, J. Phys. Chem. A **102**, 8827 (1998).
[32] A. Sanov, S. Nandi, K. D. Jordan, and W. C. Lineberger, J. Chem. Phys. **109**, 1264 (1998).
[33] A. Sanov and W. C. Lineberger, PhysChemComm **5**, 165 (2002).
[34] T. Sanford, S. Y. Han, M. A. Thompson, R. Parson, and W. C. Lineberger, J. Chem. Phys. **122**, 054307 (2005).
[35] T. Habteyes, L. Velarde, and A. Sanov, Chem. Phys. Lett. **424**, 268 (2006).
[36] R. Zadoyan, Z. Li, C. C. Martens, and V. A. Apkarian, J. Chem. Phys. **101**, 6648 (1994).
[37] A. Sanov, T. Sanford, S. Nandi, and W. C. Lineberger, J. Chem. Phys. **111**, 664 (1999).
[38] J. F. Arenas, J. C. Otero, D. Peláez, and J. Soto, J. Chem. Phys. **122**, 084324 (2005).
[39] A. M. Wodtke, E. J. Hintsa, and Y. T. Lee, J. Phys. Chem. **90**, 3549 (1986).
[40] J. F. Arenas, J. C. Otero, D. Pelaez, and J. Soto, J. Chem. Phys. **119**, 7814 (2003).
[41] D. F. McMillen and D. M. Golden, Annu. Rev. Phys. Chem. **33**, 493 (1982).
[42] K. M. Ervin, J. Ho, and W. C. Lineberger, J. Phys. Chem. **92**, 5405 (1988).
[43] K. R. Lykke, K. K. Murray, D. M. Neumark, and W. C. Lineberger, Philos. Trans. R. Soc. London, Ser. A **324**, 179 (1988).
[44] Using the RRKM theory, we estimate the autodetachment timescale of NM^- with an internal energy of 3.5 eV to be in excess of 1 ps.
[45] A. W. Castleman and K. H. Bowen, J. Phys. Chem. **100**, 12911 (1996).
[46] A. Sanov and W. C. Lineberger, Phys. Chem. Chem. Phys. **6**, 2018 (2004).